

Low temperature melting of copper nanorod arrays

Tansel Karabacak,^{a)} James S. DeLuca, and Pei-I Wang

*Department of Physics, Applied Physics and Astronomy, Rensselaer Polytechnic Institute,
Troy, New York 12180-3590*

Gregory A. Ten Eyck

*Department of Electrical, Computer, and Systems Engineering, Rensselaer Polytechnic Institute,
Troy, New York 12180-3590*

Dexian Ye, Gwo-Ching Wang, and Toh-Ming Lu

*Department of Physics, Applied Physics and Astronomy, Rensselaer Polytechnic Institute,
Troy, New York 12180-3590*

(Received 16 August 2005; accepted 3 February 2006; published online 20 March 2006)

We report the melting of nanorod arrays of copper at temperatures much lower than its bulk melting point (1083 °C). The Cu nanorods were produced by an oblique angle sputter deposition technique through a physical self-assembly mechanism due to the shadowing effect. The as-deposited nanorods were ~ 2300 nm in length, ~ 100 nm in diameter, and separated from each other with gaps varying between ~ 10 and ~ 30 nm. The melting process was investigated through the analysis of scanning electron microscopy, transmission electron microscopy, and x-ray diffraction measurements. Start of premelting (or surface melting) has been observed to occur at annealing temperature ~ 400 °C under vacuum (10^{-6} Torr). As the temperature was raised the arrays of Cu nanorods started to coalesce and formed a dense continuous film with a (111) texture at ~ 550 °C. The results of this work may be useful for low temperature soldering applications. © 2006 American Institute of Physics. [DOI: [10.1063/1.2180437](https://doi.org/10.1063/1.2180437)]

I. INTRODUCTION

Melting of crystalline materials is a common phenomenon and can be characterized by the losing of crystal order followed by a transformation to liquid phase. Recently, it has been realized that the melting behavior of nanometer-size particles can be quite different from that of bulk materials (see Refs. 1–6 and references therein). For this reason, the subject has attracted great interest among researchers and many important findings about the melting of nanostructures have been revealed. It has been reported that the melting of nanostructures is initiated with an enhanced surface diffusion. When the particle size is reduced, the ratio of surface to volume increases along with the surface curvature. This makes the atoms at the outer surface more prone to detach from their positions and diffuse on the surface as adatoms. This process can lead to a change in the shape^{2,7} of the particle at relatively low temperatures compared with the bulk melting point of the elemental material. Surface diffusion is followed by a partial melting of the nanostructure mainly within a thin layer close to the surface, which is called “surface melting” or “premelting.”⁸ The premelting generally occurs at temperatures much lower than the bulk melting point but the detailed values depend on the parameters such as size^{1,9} and morphology¹⁰ of the nanostructure, existence of impurities,¹¹ defects,⁷ strain,² and also crystallographic orientation at the surface.^{1,2} Finally, similar to the premelting, the interior melting of a nanoparticle can take place at temperatures lower than the bulk melting point. During premelting and interior melting, a particle generally changes its

shape (e.g., rod to sphere) in order to minimize the surface to volume ratio and therefore minimize its surface energy.

In some cases, the melting behavior has been realized to differ from particle to particle that were produced during the same experiment. For example, Lisecki *et al.*¹² reported that individual nanorods of copper, which were obtained by a solution based chemical synthesis method, melted at temperatures close to the bulk melting point of 1083 °C. However, some of the Cu nanorods (of ~ 20 nm in diameter and ~ 1000 nm in length) they studied showed a premelting at temperatures close to 450 °C that was associated with a shape change to shorter lengths and larger diameters. They attributed the premelting to the defects that were believed to be in the form of either dislocations or stacking faults.

In all the previous studies the nanoparticles investigated were produced in relatively small amounts and also they were isolated from each other. Therefore, after melting, the particles either changed their shapes or coalesced with a few others. The volumes of melted and coalesced particles were not large enough to form much bigger particles or continuous thin films. In this work, we report the low temperature surface and interior melting of copper nanorod arrays that resulted in a continuous dense Cu film. The nanorods are grown on large area substrates using an oblique angle sputter deposition technique.^{13,14} Our results may be useful for low temperature and large area soldering applications.¹⁵

II. EXPERIMENT

In our experiment, an oblique angle, dc magnetron sputtering system was used to deposit the Cu nanorods. Details of the experimental setup have been described elsewhere.¹³

^{a)}Electronic mail: karabt@rpi.edu

The depositions were performed on ~ 300 nm thick amorphous silicon nitride films coated on *p*-Si(100) (resistivity of 12–25 Ω cm) substrates ($\sim 3 \times 4$ cm² size) using a 99.95% pure Cu cathode (diameter of ~ 7.6 cm). The silicon nitride was deposited by a plasma enhanced chemical vapor deposition system and this layer was used to minimize Si impurity effect¹¹ on the melting of copper nanorods at the interface. The distance between the substrate and cathode was ~ 18 cm. During the growth, the substrate was tilted so that the angle between the surface normal of the substrate and the surface normal of the target was $\sim 85^\circ$. The base pressure of $\sim 4 \times 10^{-7}$ Torr was achieved using a turbomolecular pump backed by a mechanical pump. In all the sputter deposition experiments, the power was 200 W with an ultrapure Ar pressure of 2.0 mTorr. The deposition rates were measured to be ~ 46 nm/min for normal incidence and ~ 8 nm/min for oblique angle incidence as determined by a step profilometer and also verified by scanning electron microscopy (SEM) cross-sectional images. For our experiment, no intentional heating was applied to the substrate and the maximum temperature of the substrate during the deposition was measured by *K*-type thermocouple wires mounted to the back of the substrate to be $\sim 85^\circ\text{C}$.

The annealing of copper samples was performed in a minilamp annealing system (MILA-3000, Ulvac/Sinku-Riko Inc., Chigasaki, Japan). The base pressure of $\sim 1 \times 10^{-6}$ Torr was achieved using a diffusion pump backed by a mechanical pump. In order to protect the annealing system from the coating of evaporated copper during annealing, the samples were kept in a quartz box that was closed with a lid on the top. The design of this box allows the lid of the box to be discarded and replaced easily if the accumulated Cu coating on the lid cuts down the radiation heating of the sample placed inside the box from the lamp. A *K*-type thermocouple was inserted into the box through a slit and was in contact with the copper surface for sample temperature measurement. The system can provide reliable annealing to $\sim 1200^\circ\text{C}$. The temperature ramp-up rate was $\sim 33^\circ\text{C}/\text{min}$. Due to the high thermal conductivity of the copper and the Si substrate, the heating rate used was expected to provide a uniform annealing of both the surface and the interior of the Cu rods. The samples were kept at a desired annealing temperature for 30 min, then followed by a cooling step with a ramp-down rate of $\sim 17^\circ\text{C}/\text{min}$. Separate samples were annealed at various temperatures (*T*) ranging from 300 to 800 $^\circ\text{C}$ with $\sim 50^\circ\text{C}$ increments.

The annealed Cu rods were imaged by a field emission SEM (FESEM-6330F, Jeol Ltd., Tokyo, Japan). The distance between the sample and the objective lens was ~ 15 mm during the imaging. The accelerating voltage was 5 kV and the current through the tungsten emitter was 12 μA . The crystal texture information of the samples was characterized by x-ray diffraction (XRD) using a Scintag diffractometer with a Cu $K\alpha_1$ x-ray beam operated at 50 kV and 30 mA. The wavelength of the Cu $K\alpha_1$ x-ray beam was 1.540 56 \AA . The diffractometer was calibrated with respect to the peak positions of a Si calibration standard. The θ - 2θ XRD scans were performed at an angular step of 0.01° with a scan rate of $0.5^\circ/\text{min}$. Transmission electron microscopy (TEM) of indi-

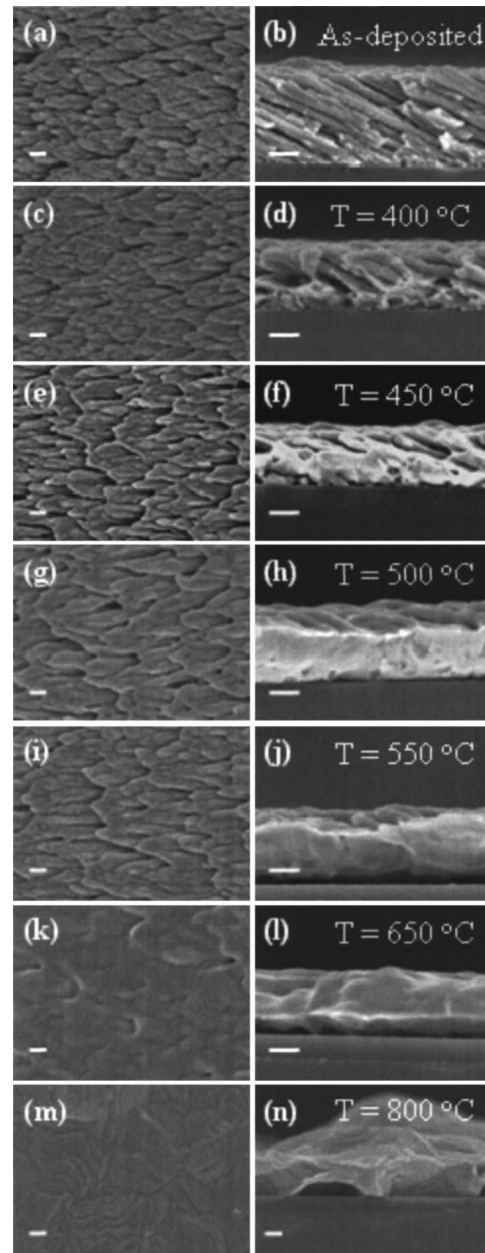


FIG. 1. The top-view (left column) and cross-sectional SEM view (right column) of copper nanorod arrays annealed at various temperatures. A different sample was used for each annealing temperature. Premelting starts at $\sim 400^\circ\text{C}$ and a continuous film is formed at $T > 550^\circ\text{C}$. The scale bars shown are 300 nm.

vidual nanorods was carried out using a Philips CM-12 microscope operating at 120 kV and 10 μA . The Cu rods were removed from the substrate by a razor blade and then dispersed onto the lacy carbon film on a Cu grid (from Ernest F. Fullam, Inc.) for the TEM investigation.

III. RESULTS AND DISCUSSION

A. Annealing temperature dependent morphology of nanorod arrays

Figures 1(a) and 1(b) show the top and cross-sectional SEM images of as-deposited copper rods, respectively. As can be seen the rods are tilted towards the incident oblique angle flux. The tilt angle is $\sim 64.5^\circ \pm 0.6^\circ$ as measured from

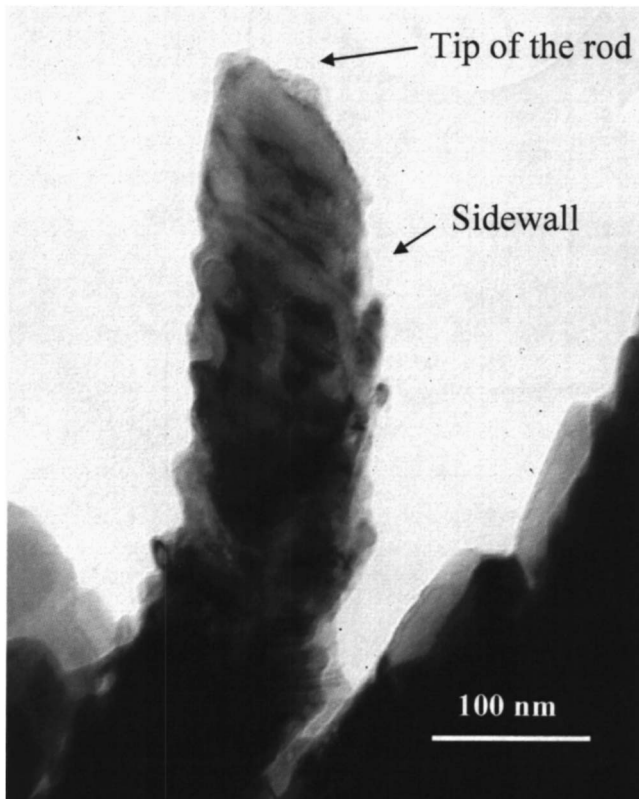


FIG. 2. TEM image of an individual as-deposited copper rod reveals that the sidewall of the rod is rough.

the surface normal. The as-deposited nanorods are ~ 2300 nm in length, ~ 100 nm in diameter, and are separated from each other with gaps varying between ~ 10 and 30 nm. The thickness of the rods layer is ~ 1000 nm. The TEM image in Fig. 2 reveals that the individual nanorods are “rough.” The rods have finer features with sizes ranging from about 1 to 10 nm, branching out from their sidewalls.

From 300 up to 400 °C annealing temperature, no significant change in the nanorods is observed from the SEM images (not shown). However, starting at $T=400$ °C the rods start to go through a morphological change where they appear to fuse to each other, as can be seen in Figs. 1(c) and 1(d). This becomes even clearer at higher annealing temperatures up to ~ 550 °C [Figs. 1(e)–1(j)]. The nanorod arrays coalesce and result in a densification of the structure. The densification is also associated with the change in the rod tilt angle of the rods. As measured from the SEM images, Fig. 3 plots the rod tilt angle as a function of the annealing temperature. More cross-sectional SEM images in addition to Fig. 1 have been used in order to measure the average tilt angle of ~ 10 rods from the sample annealed at a given annealing temperature. It is realized that the rods gradually collapse towards the substrate starting from the as-deposited tilt angle value of $64.5^\circ \pm 0.6^\circ$ to $74.1^\circ \pm 3.7^\circ$ at $T=550$ °C. The change of the tilt angle seems to be a linear function of the annealing temperature. As the rods start to collapse, a reduction in the thickness of the rods layer is observed from the cross-sectional SEM images of Fig. 1. However, we note that the observed thickness change may also be partially due to the nonuniformity of thickness across the substrate surface in oblique angle deposited films.

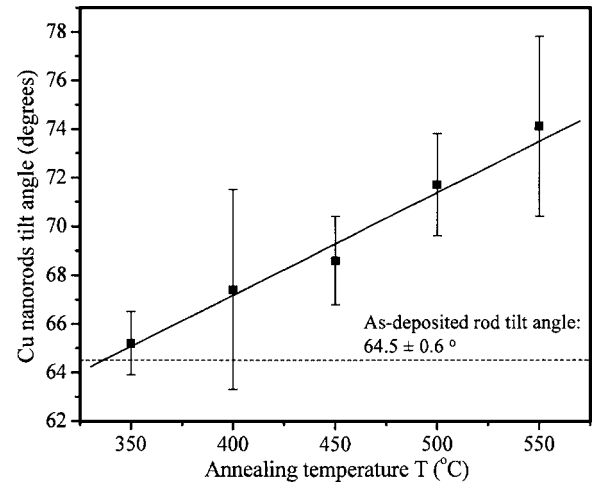


FIG. 3. Plot of the change of Cu nanorods tilt angle as a function of annealing temperature. The straight line is a linear fit to data. The as-deposited rods has a tilt angle of $64.5^\circ \pm 0.6^\circ$ and they gradually change to $74.1^\circ \pm 3.7^\circ$ at $T=550$ °C before completely collapsing.

As annealing temperatures go above 550 °C, more drastic changes occur. The nanorods start to disappear and form a uniform thin film as a result of coalescence. For example, as shown in Figs. 1(k) and 1(l) for $T=650$ °C, the structure becomes a continuous film with a rough surface. It becomes even more dense at higher temperatures of ~ 800 °C [Figs. 1(m) and 1(n)]. The surfaces of these high temperature films show faceted terrace structures [e.g., Fig. 1(m)], which is an indication of recrystallization. For the samples annealed at temperatures close to 800 °C, it has been observed to partially delaminate from the substrate in the form of a film. Figure 1(n) also shows the delaminated sections of the sample annealed at 800 °C.

The morphological change observed in the SEM images of the annealed rods is also reflected in their Fourier space spectrum. Figure 4 shows the power spectral density (PSD) profiles at various annealing temperatures obtained from the SEM images in Fig. 1. In Fig. 4, PSD 1D_x and PSD

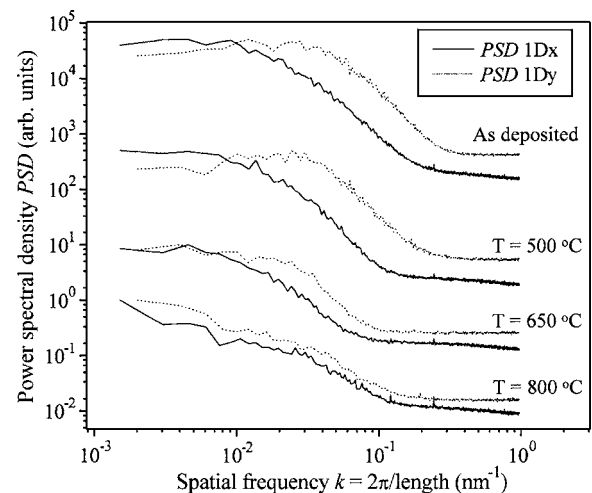


FIG. 4. One-dimensional power spectral density (PSD) functions measured along the x (horizontal) and y (vertical) directions of the SEM images in Fig. 1. The profiles were normalized and offset for clarity. The anisotropy along the x and y directions decreases as the annealing temperature is increased.

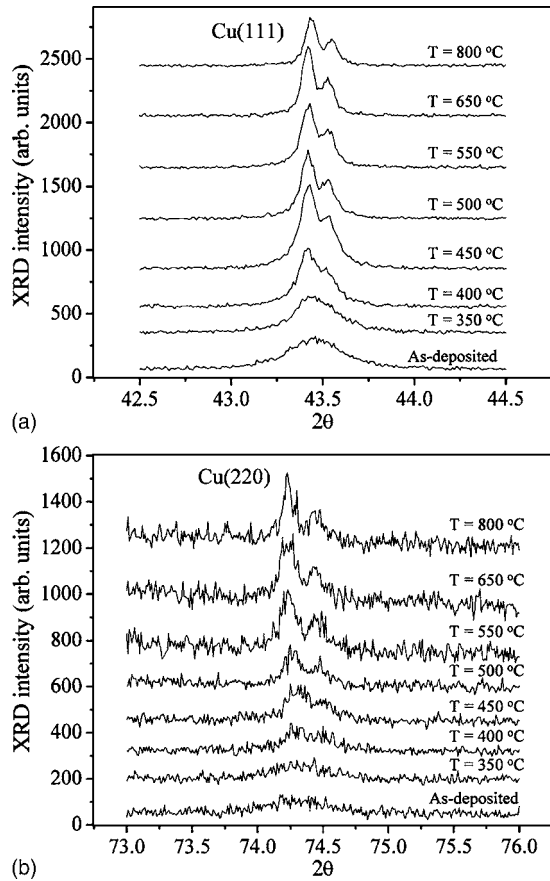


FIG. 5. Plot of the evolution of Cu(111) and Cu(220) XRD peaks from θ - 2θ spectra measured from nanorod samples at various annealing temperatures. The peaks become stronger in intensity and narrower in width at annealing temperatures $T > 400$ °C. The formation of satellite peaks is also observed at higher 2θ angles.

1Dy represent the one-dimensional Fourier transform of the surface heights (in our case brightness intensity of arbitrary units) along the horizontal and vertical directions in the SEM images of Fig. 1, respectively. The PSD spectrum of the as-deposited nanorods along the y direction is wider and extends to higher spatial frequencies. This is consistent with the anisotropic morphology of the rods where they are elongated and more closely spaced along the y direction. The anisotropy originates from the one-dimensional shadowing effect that is due to the directional grazing flux of Cu atoms along

the x axis. As the annealing temperature is increased, the anisotropy in the PSD profiles of Fig. 4 along the x and y directions starts to disappear. The change in the PSD spectra are significant at annealing temperatures close to ~ 650 °C, which is consistent with the formation of a relatively isotropic and continuous film at these temperatures.

B. Annealing temperature dependent structures of nanorod arrays and film

In addition to the qualitative observations from the SEM images, further insight into the structural changes of the annealed Cu nanorod arrays can be obtained by XRD analysis. The recrystallization of the melting should be reflected in the intensity changes of the texture peaks in XRD. Figures 5(a) and 5(b) are plots of the Cu(111) and Cu(220) peaks as a function of annealing temperature, respectively. Table I summarizes the peak position values obtained from the XRD spectra. The as-deposited Cu nanorods have a weak Cu(111) texture normal to the surface located at $2\theta \sim 43.46^\circ \pm 0.01^\circ$, while the (220) peak located at $\sim 74.29^\circ \pm 0.02^\circ$ is almost absent. This is due to the tilted texture from the substrate normal as a result of shadowing during oblique angle deposition.¹⁶ These peak positions are slightly larger than their equilibrium values of 43.30° and 74.13° for the Cu(111) peak and the Cu(220) peak, respectively. This corresponds to a lattice constant ~ 3.606 Å, that is $\sim 0.25\%$ smaller than the equilibrium value of 3.615 Å. We believe this is due to a tensile stress in the nanorod layer that reduces the lattice constant and pushes the XRD peaks to larger 2θ positions. The tensile stress can originate from the voids and defects associated with the shadowing effect during oblique angle deposition. It can also be a result of thermal stress induced from the mismatch between thermal expansion coefficients of the substrate and the film.

No significant change was observed until $T=400$ °C. When the annealing temperature exceeded 400 °C, the (111) peak shifted to a smaller 2θ ($\sim 43.42^\circ \pm 0.01^\circ$), closer to its equilibrium position, and became stronger in intensity and narrower in width. Also, the Cu(220) peak started to appear ($2\theta \sim 74.23^\circ \pm 0.01^\circ$) especially at $T > 400$ °C. These spectra indicate recrystallization and the formation of larger grains during annealing. Note that the satellite peaks seen in both the Cu(111) and Cu(220) plots in Fig. 5 originate from

TABLE I. The θ - 2θ XRD peak positions of Cu(111) and Cu(220) from nanorod array and conventional Cu samples are summarized. The equilibrium 2θ values for Cu(111) and Cu(220) peaks are 43.30° and 74.13° , respectively, which corresponds to a lattice constant of 3.615 Å. The calculated amounts of reduction in the lattice constant with respect to the equilibrium value are also listed.

Sample	XRD Cu(111) 2θ peak position (°)	XRD Cu(220) 2θ peak position (°)	Reduction in the lattice constant (compared with 3.615 Å) (%)
As-deposited Cu nanorods	43.46 ± 0.01	74.29 ± 0.02	0.25
Cu nanorods after annealing ($T > 400$ °C)	43.42 ± 0.01	74.23 ± 0.01	0.22
As-deposited Cu film	43.35 ± 0.01	N/A	0.08
Cu film after annealing ($T = 450$ °C)	43.34 ± 0.01	N/A	0.06

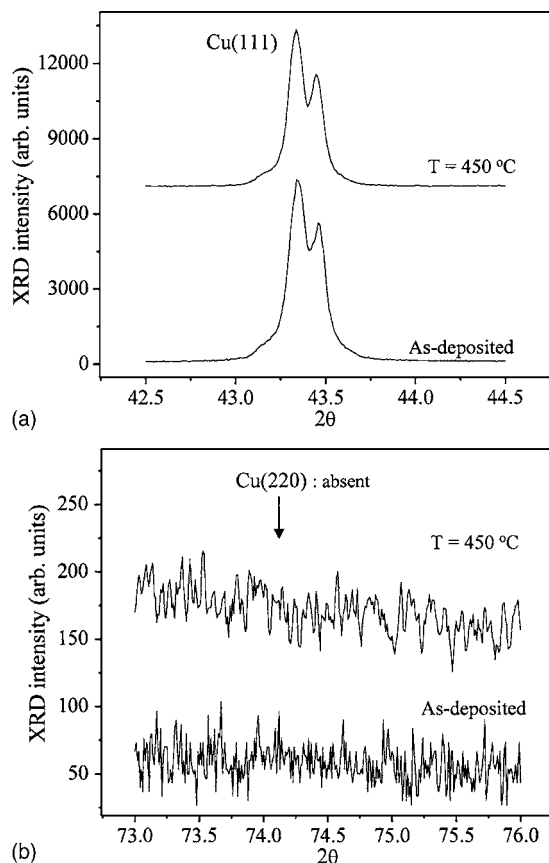


FIG. 6. XRD θ - 2θ plots measured from a conventional flat Cu film before and after annealing at $T=450$ °C. There is no significant change in the (111) texture after annealing.

the x-ray beam that consists of $K\alpha_1$ and $K\alpha_2$ energies. Cu $K\alpha_2$ has a longer wavelength of 1.544 39 Å compared with the $K\alpha_1$ of 1.540 56 Å. The $K\alpha_2$ gives rise to the satellite peaks located 0.10° to the right of $K\alpha_1$. These satellite peaks are generally observed in measurements of large crystals, further suggesting the formation of larger grains in the annealed Cu nanorods as a result of a recrystallization process.

As a comparison to the nanorod samples, we also annealed the conventional Cu films of ~ 700 nm thickness, deposited at normal incidence using the same sputtering system. The substrate was a silicon wafer with a native oxide layer. Figure 6 shows the XRD results before and after annealing the Cu film sample at $T=450$ °C. This temperature value was chosen because the previous nanorod samples started to show significant premelting characteristics at ~ 450 °C. The as-deposited conventional film shows a strong Cu(111) texture at $2\theta \sim 43.35^\circ \pm 0.01^\circ$ and the (220) is absent down to the noise level. The Cu(111) peak position is closer to the equilibrium position of 43.30° compared with that of the nanorods ($\sim 43.46^\circ$). This corresponds to a small tensile stress with a lattice constant value of ~ 3.612 Å, that is $\sim 0.08\%$ smaller than the equilibrium value. The larger tensile stress in the Cu nanorods compared with that in the Cu film (deposited at similar conditions) further suggests that the stress in rods mainly originates from the voids formed during oblique angle growth. However, unlike nanorods, the XRD peak intensities of the Cu film do not change as a result

of annealing. After being annealed at 450 °C, the intensity of the (111) peak does not increase and the (220) peak is still absent [the slight decrease in the (111) peak intensity is due to the smaller sample size used]. These results suggest that the copper film does not go through any significant surface diffusion or recrystallization at annealing temperatures similar to those used on the nanorod samples.

C. Origins of low temperature melting of nanorod arrays

Based on the results of SEM and XRD measurements presented above, we can sort out several temperature regimes that the copper nanorods go through before they completely melt. The first one is the low annealing temperature region $T < 400$ °C in which neither the SEM nor XRD shows any significant change in the structure of the rods. At annealing temperatures $T \sim 400$ – 550 °C, the nanorods start to coalesce and form a denser film, which is associated with the recrystallization and formation of larger grains.⁸ The collapse of the rods that was observed from the tilt angle change and the small separation among rods (~ 10 – 30 nm) further help the rods to fuse with each other. These results are consistent with the previous observations by Wang *et al.*² where they also observed surface diffusion followed by premelting and coalescence of Pt nanoparticles at temperatures ~ 600 °C. In contrast, a conventional copper film grown by normal incidence deposition does not show any indication of significant surface diffusion or premelting at similar temperatures of ~ 450 °C.

The enhanced surface diffusion and low temperature premelting in our Cu nanorods are believed to be mainly due to their high surface/volume ratio. The small diameter (~ 100 nm) of the rods allows a large portion of the copper atoms to be positioned at the surface. Due to the high surface curvature and tension, these surface atoms can detach more easily from their equilibrium positions and start to diffuse at low temperatures (~ 400 °C), thus leading to the premelting. The finer roughness at the scale of about 1–10 nm at the sidewalls of the nanorods (Fig. 2) can further help the initiation of premelting. Although there are several models that have been explored to address the melting temperature depression observed in nanoparticles, none seem particularly well suited for the features presented in this work. Jackson and McKenna applied the Gibbs-Thompson equation to predict the melting point reduction of organic materials confined in porous solids,⁶ and similarly Chushak and Bartell have assessed the models of Pawlow¹⁷ and Sambles¹⁸ to address the melting point reduction of gold nanoclusters.⁴ The application of these models to the current phenomenon is difficult, however, because these models assume a single size object, as opposed to the nanorods in this work that possess highly varied topologies and can be viewed as groupings of many quasi-independent structures. In fact, for single size nanoparticles, the melting point reduction predicted by these models only becomes significant for features below 5 nm. However, the influence of melting nanofeatures on somewhat larger objects (10–100 nm in size) has not been studied, and this must play a role in the observed melting behavior of our Cu

nanorods. Due to the smaller diameter and spacing of the nanorods near the substrate side [see Fig. 1(b)], they are believed to start melting from the bottom instead of from the top surface. In fact, at temperatures above 400 °C, we start seeing significant changes in the tilt angle of the rods, cross-sectional SEM images, and also intensities in the XRD profiles. Additionally, the surface texture appears to fade above 400 °C, believed to be the result of the highly varied topology in the 1–5 nm range. On the other hand, the general shape of the top of the rods does not drastically change until temperatures ~ 550 °C as observed from top-view SEM images and PSD analysis. These results are suggestive of several stages of melting, all depending on the relative size of the feature examined. The combination of these effects can account for the significant melting point depression observed for rods on the order of 100 nm.

Possible defects in the rods may also play a role in the premelting.⁷ These defects can be either in the form of voids due to the shadowing effect or interstitial atoms (e.g., Cu or Ar) that originate from the penetration of energetic particles during a typical sputter deposition (e.g., ~ 1 –10 eV). As obtained from the XRD peak shifts, the tensile stress observed in the Cu nanorod array samples supports the existence of voids that formed during oblique angle growth.

At higher temperatures $T > 550$ °C, the rods disappear and they start to form a continuous film. The rods melt completely in this temperature regime. Instead of transforming to isolated shapes during melting, they collapse and fuse with each other to form a denser film due to the small gaps between nanorods. At a temperature ~ 650 °C, the film is dense but has a rough surface. However, at ~ 800 °C it becomes both very dense and smooth.

IV. CONCLUSION

We presented the melting of copper nanorod arrays at temperatures much lower than the bulk melting point. The Cu nanorods were grown by an oblique angle sputter deposition technique. The melting process starts with the surface

diffusion and premelting at ~ 400 °C, and results in the shape change and coalescence of the nanorods. At higher annealing temperatures > 550 °C, the rods start to fuse with each other and form a denser, continuous, and (111) textured thin film. The results of this work may have useful applications in low temperature soldering of materials.¹⁵

ACKNOWLEDGMENTS

This work was supported by MARCO, DARPA, and New York State. The authors J.S.D. and G.A.T.E were supported by Rensselaer Undergraduate Research Participation Program and Department of Education, respectively.

¹M. Dippel, A. Maier, V. Gimple, H. Wider, W. E. Evenson, R. L. Rasera, and G. Schatz, *Phys. Rev. Lett.* **87**, 095505 (2001).

²Z. L. Wang, J. M. Petroski, T. C. Green, and M. A. El-Sayed, *J. Phys. Chem. B* **102**, 6145 (1998).

³M. Alcoutlabi and G. B. McKenna, *J. Phys.: Condens. Matter* **17**, 461 (2005).

⁴Y. G. Chushak and L. S. Bartell, *J. Phys. Chem. B* **105**, 11605 (2001).

⁵Z. Shijin, W. Shaoqing, and Y. Hengqiang, *J. Phys. Soc. Jpn.* **70**, 2953 (2001).

⁶C. L. Jackson and G. B. McKenna, *J. Chem. Phys.* **93**, 9002 (1990).

⁷S. Link, Z. L. Wang, and M. A. El-Sayed, *J. Phys. Chem. B* **104**, 7867 (2000).

⁸L. J. Lewis, P. Jensen, and J.-L. Barrat, *Phys. Rev. B* **56**, 2248 (1997).

⁹B. Wang, G. Wang, X. Chen, and J. Zhao, *Phys. Rev. B* **67**, 193403 (2003).

¹⁰J. Wang, X. Chen, G. Wang, B. Wang, W. Lu, and J. Zhao, *Phys. Rev. B* **66**, 085408 (2002).

¹¹H. Baker, *Alloy Phase Diagram*, ASM Handbook Vol. 3 (ASM International, Metals Park, 1992), p. 178.

¹²I. Lisięcki, H. Sack-Kongehl, W. Weiss, J. Urban, and M.-P. Pileni, *Langmuir* **16**, 8807 (2000).

¹³T. Karabacak, G.-C. Wang, and T.-M. Lu, *J. Vac. Sci. Technol. A* **22**, 1778 (2004).

¹⁴T. Karabacak and T.-M. Lu, in *Handbook of Theoretical and Computational Nanotechnology*, edited by M. Rieth and W. Schommers (American Scientific, Stevenson Ranch, CA, 2005), Chap. 69.

¹⁵G. T. Eyck, T.-M. Lu, T. Karabacak, D.-X. Ye, and P.-I. Wang, Low-temperature Welding with Nanostructures, U.S. Patent No. (pending).

¹⁶F. Tang, C. Gaire, D.-X. Ye, T. Karabacak, T.-M. Lu, and G.-C. Wang, *Phys. Rev. B* **72**, 035430 (2005).

¹⁷P. Pawlow, *Z. Phys. Chem., Stoechiom. Verwandtschaftsl.* **65**, 1 (1908).

¹⁸J. R. Sambles, *Proc. R. Soc. London, Ser. A* **324**, 339 (1971).